

# A lipidomic screen of hyperglycemia-treated HRECs links 12/15-Lipoxygenase to microvascular dysfunction during diabetic retinopathy via NADPH oxidase

Ahmed S. Ibrahim,<sup>\*,†,§</sup> Sally Elshafey,<sup>\*</sup> Hassan Sellak,<sup>\*\*</sup> Khaled A. Hussein,<sup>\*,†</sup>  
Mohamed El-Sherbiny,<sup>\*,††</sup> Mohammed Abdelsaid,<sup>§§</sup> Nasser Rizk,<sup>\*\*\*</sup> Selina Beasley,<sup>\*,†††</sup>  
Amany M. Tawfik,<sup>\*,†,†††</sup> Sylvia B. Smith,<sup>†,†††</sup> and Mohamed Al-Shabrawey<sup>1,\*†,††,†††</sup>

Oral Biology and Anatomy, College of Dental Medicine,<sup>\*</sup> Department of Anesthesiology and Perioperative Medicine,<sup>\*\*</sup> Ophthalmology and Culver Vision Discovery Institute,<sup>†</sup> Department of Physiology,<sup>§§</sup> and Cellular Biology and Anatomy,<sup>†††</sup> Medical College of Georgia, Georgia Regents University, Augusta, GA; Department of Clinical Biochemistry, Faculty of Pharmacy,<sup>§</sup> Department of Anatomy, Faculty of Medicine,<sup>††</sup> Mansoura University, Mansoura, Egypt; and Biomedical Science Program,<sup>\*\*\*</sup> Faculty of Science, Qatar University, Doha, Qatar

**Abstract** Retinal hyperpermeability and subsequent macular edema is a cardinal feature of early diabetic retinopathy (DR). Here, we investigated the role of bioactive lipid metabolites, in particular 12/15-lipoxygenase (LOX)-derived metabolites, in this process. LC/MS lipidomic screen of human retinal endothelial cells (HRECs) demonstrated that 15-HETE was the only significantly increased metabolite ( $2.4 \pm 0.4$ -fold,  $P = 0.0004$ ) by high glucose (30 mM) treatment. In the presence of arachidonic acid, additional eicosanoids generated by 12/15-LOX, including 12- and 11-HETEs, were significantly increased. Fluorescein angiography and retinal albumin leakage showed a significant decrease in retinal hyperpermeability in streptozotocin-induced diabetic mice lacking 12/15-LOX compared with diabetic WT mice. Our previous studies demonstrated the potential role of NADPH oxidase in mediating the permeability effect of 12- and 15-HETEs, therefore we tested the impact of intraocular injection of 12-HETE in mice lacking the catalytic subunit of NADPH oxidase (NOX2). The permeability effect of 12-HETE was significantly reduced in NOX2<sup>-/-</sup> mice compared with the WT mice. In vitro experiments also showed that 15-HETE induced HREC migration and tube formation in a NOX-dependent manner. Taken together our data suggest that 12/15-LOX is implicated in DR via a NOX-dependent mechanism.—Ibrahim, A. S., S. Elshafey, H. Sellak, K. A. Hussein, M. El-Sherbiny, M. Abdelsaid, N. Rizk, S. Beasley, A. M. Tawfik, S. B. Smith, and M. Al-Shabrawey. A lipidomic screen of hyperglycemia-treated HRECs links 12/15-Lipoxygenase to microvascular dysfunction during diabetic retinopathy via NADPH oxidase. *J. Lipid Res.* 2015. 56: 599–611.

**Supplementary key words** diabetic retinopathy • 12- and 15-HETEs • retinal vascular leakage • reduced nicotinamide adenine dinucleotide phosphate oxidase • retinal inflammation • lipoxygenase • bioactive lipids

Diabetic retinopathy (DR), the most prevalent microvascular complication of diabetes, is responsible for over 10,000 new cases of blindness every year in the United States alone (1). The risk of vision loss increases with the development of diabetic macular edema and/or retinal neovascularization (NV), the former being a direct consequence of blood-retinal barrier (BRB) dysfunction and the latter the result of widespread retinal ischemia (2).

For years, significant effort has been invested in elucidating the mechanisms that underlie destructive preretinal NV in DR (3). Nonetheless, considerably less is known about the molecular events that lead to BRB dysfunction that is characterized by enhanced retinal vascular permeability and recruitment of inflammatory cells. Moreover, existing regimens of treatment carry nonspecific adverse effects. These include increased risk of thromboembolic incidence, neuronal toxicity, and geographic atrophy with anti-vascular endothelial growth factor (VEGF) therapies

Abbreviations: AA, arachidonic acid; BCF, Bonferroni correction factor; BRB, blood-retinal barrier; DR, diabetic retinopathy; ECIS, electric cell-substrate impedance sensing; HDoHE, hydroxydocosahexaenoic acid; HG, high glucose; HREC, human retinal endothelial cell; LOX, lipoxygenase; NAC, N-acetyl-L-cysteine; NOX, NADPH oxidase; NV, neovascularization; OIR, oxygen-induced retinopathy; PLA2, phospholipase A2; PMN, polymorphonuclear leukocyte; ROS, reactive oxygen species; TER, transcellular electrical resistance; VEGF, vascular endothelial growth factor.

<sup>1</sup>To whom correspondence should be addressed.  
e-mail: malshabrawey@gru.edu

This publication was made possible by National Institutes of Health Grant 5R01EY023315 and National Priorities Research Program Grant 4-1046-3-284 from the Qatar National Research Fund (a member of Qatar Foundation). This study was also supported in part by the National Center for Research Resources, National Institutes of Health Grant S10RR027926.

Manuscript received 14 November 2014 and in revised form 15 January 2015.

Published, JLR Papers in Press, January 17, 2015  
DOI 10.1194/jlr.M056069

Copyright © 2015 by the American Society for Biochemistry and Molecular Biology, Inc.

This article is available online at <http://www.jlr.org>

(4, 5). Likewise, cumulative risks of cataract and glaucoma, as well as local immunosuppression, are frequently associated with corticosteroid intravitreal therapy (6, 7). Even with laser-based photocoagulation, the gold standard treatment for DR, side effects ranging from blurred peripheral vision to scotomas may occur (8). These therapeutic limitations impose the necessity for novel therapeutic interventions via unraveling the pathophysiology of DR.

In recent years, human studies have underscored the strong association between dyslipidemia and the development of DR. Clinically, it has been reported that the severity of retinopathy in type 1 diabetes was correlated positively with triglyceride level and negatively with the HDL concentration (9). Additionally, intensive dyslipidemia therapy significantly slowed the progression of DR in type 2 diabetes over 4 years (10). Diabetic dyslipidemia is characterized by a shift in the fatty acid profile with an increase in omega-6 PUFAs, in particular arachidonic acid (AA), released from membrane lipids by the activated phospholipase A2 (PLA2) (11, 12). The released AA, in turn, can be converted to inflammatory bioactive lipid mediators such as HETEs, leukotrienes, and prostaglandins via different enzymatic pathways including cyclooxygenase, lipoxygenase (LOX), and cytochrome P450 (13).

Bioactive lipids activate specific signaling pathways that are implicated in cell proliferation, differentiation, and apoptosis. Sustained cellular response to increased bioactive lipids becomes pathological and results in chronic diseases such as cancer and atherosclerosis (14).

While there is irrefutable evidence for the role of dyslipidemia in the progression of DR (9, 15), bioactive lipid metabolites have received limited attention. HETEs are major monohydroxylated AA bioactive lipid metabolites that are produced during inflammatory and immunological reactions (16). The 12- and 15-HETEs are formed by human 15-LOX and its murine ortholog 12/15-LOX (17) in a variety of mammalian cells such as endothelial cells, eosinophils, and epithelial cells to exhibit distinct biological activities. These activities include stimulation of endothelial cell mitogenesis, vascular inflammation, and mucus release from human airways (18–20). Recently, we have shown that pharmacological inhibition or deletion of 12/15-LOX reduces retinal NV in the oxygen-induced retinopathy (OIR) model (21). Moreover, we have demonstrated in both human patients and animal models that retinal expression of 12/15-LOX is robustly induced during diabetes (21). At the same time, its pharmacological inhibition dampened the levels of inflammatory cytokines, reactive oxygen species (ROS) generation, and phosphorylated VEGF receptor 2 expression in the retinas of diabetic mice (22). However, the cellular source of these lipid metabolites is unknown and could be derived from retinal tissues, including the retinal vascular endothelial, glial, and pigmented epithelial cells, as well as from infiltrated inflammatory cells. Moreover, the role of 12- or 15 HETE in mediating the breakdown of barrier function, such as that observed in DR, has not been investigated thoroughly to date.

In addition to dyslipidemia, oxidative stress has attracted considerable interest as a key factor in mediating retinal vascular injury during DR. Our previous studies highlighted NADPH oxidase (NOX) as a major source of ROS generation in the retinas of experimental diabetic rodents and OIR models, as well as in retinal endothelial cells treated with high glucose (HG) or hypoxia (23–26). Our recent study showed that inhibiting 12/15-LOX by baicalein reduced diabetes-induced ROS generation and NOX2 expression in mouse retina, suggesting the existence of an interconnected signaling between LOXs and NOX (22). However, the cross-talk between NOX and inflammatory bioactive lipids remains ill-defined in DR.

Therefore, the current study has been taken up to characterize the effect of hyperglycemia on bioactive-lipid profile in human retinal endothelial cells (HRECs) to determine whether endothelial cells are a potential source of 12/15-LOX-derived hydroxyeicosanoids, and whether these metabolites play a causative role in the pathogenesis of BRB dysfunction during diabetes. Furthermore, the present work aimed to gain insights into the underlying molecular mechanisms by portraying the causal relationship with NOX.

## RESEARCH DESIGN AND METHODS

### Animal preparation and experimental design

All procedures with animals were performed in accordance with the Public Health Service Guide for the Care and Use of Laboratory Animals (Department of Health, Education, and Welfare publication, National Institutes of Health 80-23) and Georgia Regents University guidelines. Six to eight-week-old male 12/15-LOX knockout ( $LOX^{-/-}$ ) mice lacking the NOX2 subunit of NOX ( $NOX2^{-/-}$ ), and corresponding littermate controls, WT mice in C57BL/6J background (Jackson Laboratory, Bar Harbor, ME), were matched according to sex, age, and weight. Animals were given intraperitoneal injections of freshly prepared streptozotocin (45 mg/kg; Enzo Life Sciences) dissolved in 0.9% NaCl after 4 h fasting for five consecutive days. Mice with blood glucose levels  $>300$  mg/dl were considered diabetic. Six weeks after establishment of diabetes, retinal vascular permeability was evaluated using fluorescein angiography. Thereafter retina samples were used for total albumin analysis by Western blot.

For intravitreal injections, the procedure was essentially the same as previously described (27). To avoid uncontrolled intraocular pressure increase, the volume of intravitreal injections was limited to 1  $\mu$ l. 12-HETE was dissolved in ethanol and a working solution of 10 $\times$  was prepared by diluting 0.32  $\mu$ l of stock solution (312  $\mu$ M) to 100  $\mu$ l with PBS, assuming the vitreous volume of mouse eye is  $\sim 10$   $\mu$ l (28). Then by injecting 1  $\mu$ l of this working solution, a 0.1  $\mu$ M vitreal concentration of 12-HETE was obtained. The vitreal concentration of ethanol was 0.032%. The volume of the injected solution apparently did not cause significant pressure-induced retinal damage, because 0.032% ethanol-PBS-injected control eyes showed normal retinal morphology with no apparent apoptosis within 7 days. The dose of 12- or 15-HETE was chosen according to what was detected previously in the vitreous of patients with DR, 50 ng/ml ( $\sim 0.1$   $\mu$ M) (21).

## Microvascular HRECs

In vitro experiments were performed using cultured HRECs (Cell Systems Corporation). After the cells were 80–90% confluent, they were serum starved (2% FBS) overnight, then treated with 15-HETE (0.1  $\mu$ M) with or without apocynin (30  $\mu$ M) or *N*-acetyl-L-cysteine (NAC) (50  $\mu$ M), or HG (D-glucose, 30 mM) in the presence or absence of 20  $\mu$ M of AA. The osmolarity of the control group in the HG experiments was adjusted using L-glucose. Cytotoxicity of tested inhibitors was assessed by MTT assay as previously described (29). Transcellular electrical resistance (TER) and cell migration were done using electric cell-substrate impedance sensing (ECIS) (Model 1600R, Applied BioPhysics) as previously described (30, 31). The experiment was terminated after 24 h of 15-HETE treatment for analysis of leukocyte adhesion and tube formation. Conditioned media were used for multiplex assay of various cytokines as previously described (30). Meanwhile, the HG experiment was terminated 5 days after initiation of treatment and cell lysates were collected and analyzed for 15-LOX and 5-LOX protein expression using Western blot analysis. At the same time, collected cell lysates were assayed for PLA2 activity according to manufacturer's instructions (Cayman, Ann Arbor, MI). For lipidomic analysis, the cells were incubated in indicator-free media for 5 days and then collected with cells together, sonicated, centrifuged to remove cell debris, and then frozen for the analysis in the Lipidomics Core Facility (Wayne State University, Detroit, MI) as described before (32).

## Immunofluorescence

Retinal paraffin sections of human subjects with or without DR obtained from Capital Bioscience (Rockville, MD) were fixed in 10% neutral buffered formalin. Following rehydration of the paraffin section and two washes in PBS, sections were treated with proteinase K for 10 min and washed twice in PBS followed by blocking with 10% normal goat serum and then incubated with phospho-PLA2 antibody overnight in a humidified container at

4°C. The next day the sections were incubated in Oregon green-labeled anti-rabbit antibody. Sections were covered using DAPI mounting medium and images were obtained with confocal microscopy (LSM 510; Carl Zeiss).

## Fluorescein angiography

The anesthetized mouse was placed on the imaging platform of the Phoenix Micron III retinal imaging microscope and Goniovisc 2.5% was applied liberally to keep the eye moist during imaging. Mice were administered 10 to 20  $\mu$ l 10% fluorescein sodium and rapid acquisition of fluorescent images ensued for ~5 min, as previously described (33).

## Protein extraction and Western blot analysis

Cell or retinal lysates were subjected to Western blot analysis using antibodies for 15-LOX1 (Novus biologicals, Littleton, CO), 5-LOX and  $\beta$ -actin (Millipore Corporation, Billerica, MA), VCAM-1 and ICAM-1 (Cell Signaling Technology, Beverly, MA), albumin (Bethyl, TX), NOX2 (BD Biosciences, Franklin Lakes, NJ), and CD45 (Santa Cruz, CA) according to a previous procedure (27).

## RNA interference

HRECs were transfected with NOX2 or control Dicer-substrate RNA duplexes (catalog number HSC.RNAI.N000397.12, Integrated DNA Technologies) using lipofectamine 2000 per the manufacturer's instructions.

## In vitro leukocyte adhesion assay

HRECs were grown to confluence in 12-well plates then treated with or without 15-HETE (0.1  $\mu$ M) in the presence or absence of apocynin (30  $\mu$ M) or NAC (50  $\mu$ M), as well as with positive control, 10  $\mu$ g/ml of the endotoxin *Escherichia coli* lipopolysaccharide (Sigma-Aldrich, St. Louis, MO) for 24 h. Following the treatment, leukocytes (300,000–400,000 cells/well)

TABLE 1. Nondetectable lipid metabolites in the lipidomic profile of HRECs under hyperglycemia

Number	Lipid Metabolite	Number	Lipid Metabolite	Number	Lipid Metabolite
1	9-OxoOTrE	26	PGF1a	51	8,9-EpETrE
2	15d-D12,14-PGJ2	27	13,14dh-PGE1	52	16(17)-EpDPE
3	5-HEPE	28	7(S)-Maresin1	53	19(20)-EpDPE
4	12-OxoETE	29	PD1	54	D17-PGE1
5	5-oxoETE	30	4,17-DiHDoHE	55	8-isoPGF2a
6	15-OxoETE	31	7,17-DiHDPE	56	11bPGF2a
7	5,6-EpETrE	32	11dh-TXB3	57	7(8)-EpDPE
8	5(S)-HETrE	33	20-COOH LTB4	58	10(11)-EpDPE
9	15-OxoEDE	34	6-keto PGE1	59	13(14)-EpDPE
10	15(S)-HEDE	35	11dh-TXB2	60	RvD2
11	tetranor PGEM	36	TXB3	61	RvD5
12	5,6-DiHETE	37	19(R)-OH PGE2	62	RvE3
13	5(S),6(S)-DiHETE	38	6kPGF1a	63	PGA1
14	5(S),15(S)-DiHETE	39	19(R)-OH PGF2a	64	LTC4
15	Bicyclo PGE1	40	6,15-diketo PGFa	65	LTD4
16	5,6-DiHETrE	41	19(R)-hydroxy PGE1	66	LTE4
17	8,9-DiHETrE	42	RvD1	67	<i>N</i> -acetyl LTE4
18	11dh-2,3-dinor TXB2	43	8,9-EpETE	68	9-HEPE
19	2,3-dinor TXB2	44	14,15-EpETE	69	13,14dh-15k-PGF2a
20	RvE1	45	17,18-EpETE	70	11(R)-HEDE
21	LXA5	46	15-keto PGF2a		
22	15-keto PGE2	47	13,14dh-15k-PGE2		
23	PGF3a	48	15-keto PGE1		
24	20-hydroxy LTB4	49	13,14dh-15k-PGE1		
25	LXA4	50	PGE1		

DiH, dihydroxy; DoHE, docosahexaenoic acid; DPE, docosapentaenoic acid; EDE, eicosadienoic acid; Ep, epoxy; EPE, eicosapentaenoic acid; ETE, eicosatetraenoic acid; ETrE, eicosatrienoic acid; H, hydroxyl; LX, lipoxin; LT, leukotriene; OTrE, octadecatrienoic acid; PD, neuroprotectin; PG, prostaglandin; tetranor PGEM, tetranor-prostaglandin E metabolite; RV, resolvin; TX, thromboxane.

purchased from Sanguine Bioscience (Valencia, CA) and labeled with diluted LeukoTracker solution (Cell Biolab) for 60 min at 37°C, according to the manufacturer's instructions, were added to confluent monolayer HRECs and incubated for 90 min at 37°C. Immediately before the assay, nonadherent cells were removed by washing three times with RPMI-1640 medium (Life Technology, Grand Island, NY). The adherent labeled leukocytes were counted under the inverted fluorescence microscope at 480 nm/520 nm from three separate fields per well.

### In vitro endothelial tube formation on Matrigel

Tube formation assay was done as described before (34). Briefly, vehicle or 15-HETE (0.1  $\mu$ M) in the presence or absence of different inhibitors, was added to the appropriate wells and the cells were incubated at 37°C overnight. Tube formation was observed under an inverted microscope and the images were captured with a digital camera attached to the microscope. The measurement was done on three randomly chosen microscopic fields per well, and the mean of the three fields was used as a single observation. Tube formation was further quantified by measuring the total length of tube-like cells using ImageJ software.

### Data analysis

The results are expressed as mean  $\pm$  SD. Differences among experimental groups were evaluated by using the two-tailed *t*-test or one-way ANOVA. When statistical differences were observed using ANOVA, a post hoc Tukey's test was performed to determine which groups differed.

The Bonferroni correction factor (BCF), which accounts for a large number of comparisons by reducing the  $\alpha$  level as to decrease the probability of obtaining a type I error, was used when analyzing lipid metabolite profiles among groups. BCF was calculated by dividing the  $\alpha$  level (0.05) by the number of bioactive lipid metabolites detected. Because 56 individual metabolites were detected, the new  $\alpha$  value used for individual metabolites was 0.0009 (0.05/56). A new  $\alpha$  level of 0.0055 (0.05/9) was also calculated for the top 15% of metabolites which are used for further analysis by measuring their profile in the presence of exogenous AA as a substrate under hyperglycemic conditions.

Differences were considered statistically significant if  $P < 0.05$ , except for lipid metabolites, which used the  $\alpha$  values calculated from the Bonferroni correction.

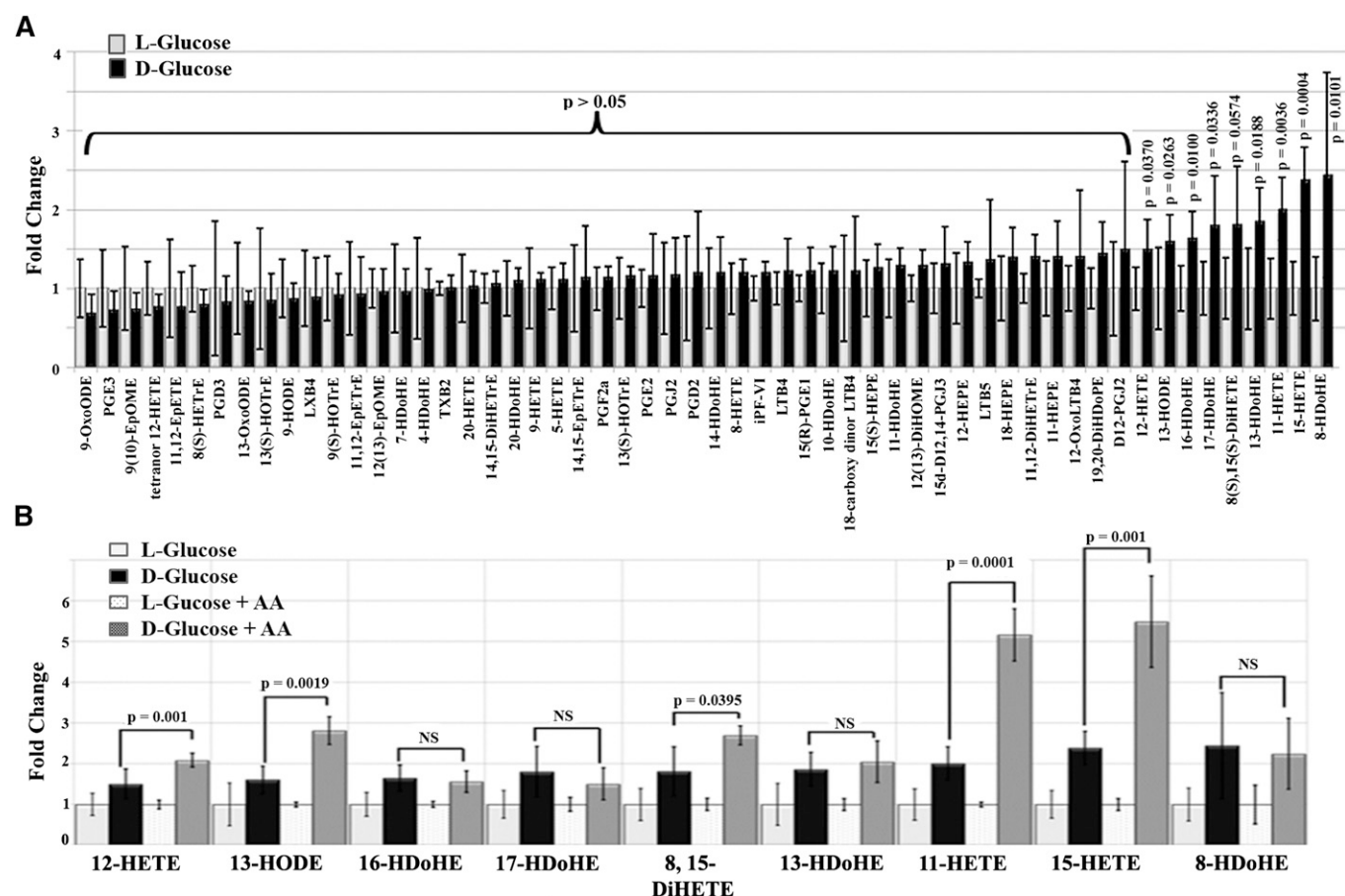


**Fig. 1.** Characterizing the effect of hyperglycemia on altering the bioactive-lipid profile in HRECs using LC/MS. **A:** Fold change in the lipidomic profile of HRECs under hyperglycemia, D-glucose (30 mM) for 5 days, compared with normo-osmotic control, D-glucose (5 mM) plus L-glucose (25 mM). **B:** Fold change of upregulated metabolites detected in the previous screen in the presence or absence of exogenous AA (20  $\mu$ M) under hyperglycemia compared with the corresponding controls, D-glucose (5 mM) plus L-glucose (25 mM), with or without AA (20  $\mu$ M). Data shown are the mean  $\pm$  SD of three independent experiments. DiH, dihydroxy; DoHE, docosahexaenoic acid; DoPE, docosapentaenoic acid; EDE, eicosadienoic acid; Ep, epoxy; EPE, eicosapentaenoic acid; ETE, eicosatetraenoic acid; ETrE, eicosatrienoic acid; H, hydroxyl; IP, isoprostane; LT, leukotriene; LX, lipoxin; ODE, octadecadienoic acid; OME, octadecenoic acid; OTrE, octadecatrienoic acid; PG, prostaglandin; TX, thromboxane.

## RESULTS

### Hyperglycemia alters bioactive-lipid profile in HRECs

In order to evaluate the potential role of bioactive lipids in mediating the edematous phenotype observed in DR, we first sought to characterize their profile under diabetic milieu. In this regard, the lipidomic profile of HRECs was screened for metabolites whose levels changed dramatically during hyperglycemia. Out of 126 bioactive lipids screened, 70 were not detectable (Table 1), 47 did not change significantly (*t*-test,  $P > 0.05$ ), and 9 metabolites were increased (*t*-test,  $P < 0.05$ ) under hyperglycemic conditions (30 mM D-glucose) compared with the normo-osmotic control (5 mM D-glucose + 25 mM L-glucose) (Fig. 1A). However, after the Bonferroni correction, the fold changes in the level of eight metabolites among the nine increased were statistically not significant, and only 15-HETE had a significant fold increase ( $2.4 \pm 0.4$ ) with a *P* value of 0.0004 (BCF  $\alpha = 0.0009$ ). Next, we narrowed our focus to confirm these data, considering the top 15% of the upregulated metabolites detected in this screen. By measuring their profile in the presence of exogenous AA as a substrate under hyperglycemic conditions, we found

a significant increase in AA-derived eicosanoids generated by the 12/15-LOX pathway including: 15-HETE (BCF  $\alpha = 0.0055$ , Tukey's post hoc,  $P = 0.001$ ), 11-HETE (BCF  $\alpha = 0.0055$ , Tukey's post hoc,  $P = 0.0001$ ), and 12-HETE (BCF  $\alpha = 0.0055$ , Tukey's post hoc,  $P = 0.001$ ) in which 15-HETE again had the highest ( $5.48 \pm 1.12$ ) fold increase. On the other hand, the levels of other non-AA-derived metabolites [8-, 13-, 16-, and 17-hydroxydocosahexaenoic acid (HDoHE) and 13-HODE] did not change significantly in the presence of exogenous AA with the exception of 13-HODE, Fig. 1B.

Western blot analysis of LOXs from HRECs further corroborated data obtained by LC/MS metabolite measurement. Results revealed that 15-LOX protein expression was significantly increased by 2.5-fold after treating HRECs with HG compared with control. Meanwhile, the protein expression level of 5-LOX did not change significantly under the same treatment, Fig. 2A. Given the prominent increase in levels of 15-HETE under the hyperglycemia, we proceeded to investigate the propensity of 15-HETE to disrupt vascular barrier function in the HREC monolayer using real-time analysis of TER, an indicator of monolayer integrity. We tested the concentration of 15-HETE

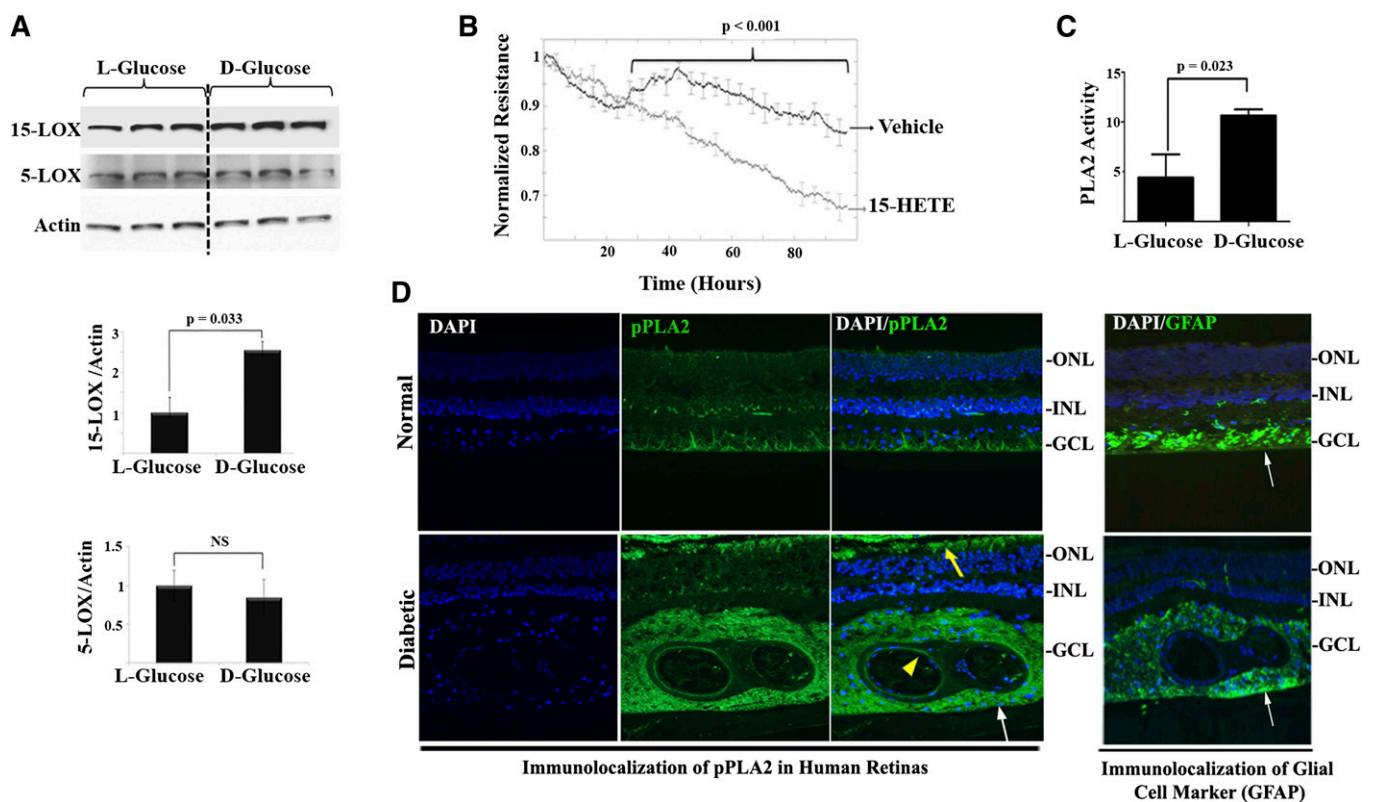


**Fig. 2.** Hyperglycemia induced 15-LOX protein expression as well as PLA2 activity. **A:** HRECs were treated with HG, D-glucose (30 mM), or normo-osmotic control for 5 days. Western blot was performed as described in the Research Design and Methods using 15-LOX, 5-LOX, and actin antibodies followed by densitometric analysis. Ratio of the band intensity of 15-LOX or 5-LOX relative to the actin was reported as fold increase in relation to normo-osmotic control (L-glucose), which was arbitrarily set at 1.0. **B:** HRECs were treated with 15-HETE or vehicle and the change in the resistance was monitored as described in Research Design and Methods using ECIS. Normalized TER for 15-HETE treatment was compared with vehicle-treated endothelial monolayer. **C:** Treatment of HRECs with D-glucose (30 mM) for 5 days stimulated the activity of PLA2 compared with normo-osmotic control. Data shown are the mean  $\pm$  SD of three independent experiments. **D:** In vivo detection of phosphorylated PLA2 (pPLA2) (active form) in serial sections from human diabetic or normal retinas around blood vessel regions (yellow arrowhead), perivascular in the area of glial cells, detected by its marker, glial fibrillary acidic protein (GFAP) (white arrows), as well as in the outer segment of the photoreceptors (yellow arrow).

that had been detected in the vitreous of patients with DR,  $\sim 55$  ng/ml (0.1–0.3  $\mu$ M) (21) and shown by us to elicit transcellular leakage of FITC-dextran in bovine retinal endothelial cells (22). Changes in TER were first observed after 26 h of 15-HETE treatment and continued to decrease throughout the experiment period, Fig. 2B.

These data presumably reflect a PLA2-dependent pathway in releasing endogenous free AA as the mediator's precursor followed by the activation of metabolizing LOXs. To this end, we determined the *in vitro* endothelial PLA2 activity in response to diabetic conditions. As depicted in Fig. 2C, treatment of HRECs with hyperglycemia for 5 days stimulated the activity of PLA2 by 2-fold compared with control. This finding of increased PLA2 activity has been substantiated by the detection of phosphorylated PLA2 (active form) in diabetic human retinal sections (Fig. 2D). Phosphorylated PLA2 was mostly localized in the endothelial layer of the retinal vessels and perivascular retinal glial cells, as well as in the outer segment of the photoreceptors.

### Evolving role of 12/15-LOX pathway in compromising retinal barrier function during diabetes

The aforementioned data from lipidomic analysis provide a rationale to explore the role of the 12/15-LOX pathway in diabetes-induced BRB breakdown. We used

two complementary approaches for this investigation. The first approach was aimed to assess whether knocking out retinal 12/15-LOX, an ortholog of human 15-LOX1 (17), would efficiently reduce the pathological vascular permeability seen in DR. To achieve this goal, we used the well-defined 12/15-LOX (Alox15) knockout mice and matched congenic controls. First, these mice were re-genotyped before the study to ensure that they had deletion of 12/15-LOX in the retina according to the Jackson Laboratory's protocol (data not shown). Next, streptozotocin was administered to  $\sim 6$ -week-old mice and blood glucose was monitored. Mice were considered diabetic if their non-fasted glucose level was higher than 300 mg/dl. After 6 weeks, the magnitude of retinal vascular leakage was assessed via a clinical diagnostic technique, fluorescein angiography. At this time point, fluorescein angiography from WT diabetic mice exhibited a significant elevation, almost 2.5-fold in fluorescein hyper-fluorescence compared with the nondiabetic littermates. In contrast, the increase in fluorescein hyper-fluorescence was significantly lowered to 1.9-fold by knocking out 12/15-LOX, Fig. 3A. To further confirm the role of the 12/15-LOX pathway in mediating diabetes-induced vascular permeability, Western blot analysis of total retinal albumin was performed. As shown in Fig. 3B, the total retinal albumin content in diabetic WT mice was 4-fold higher than that in

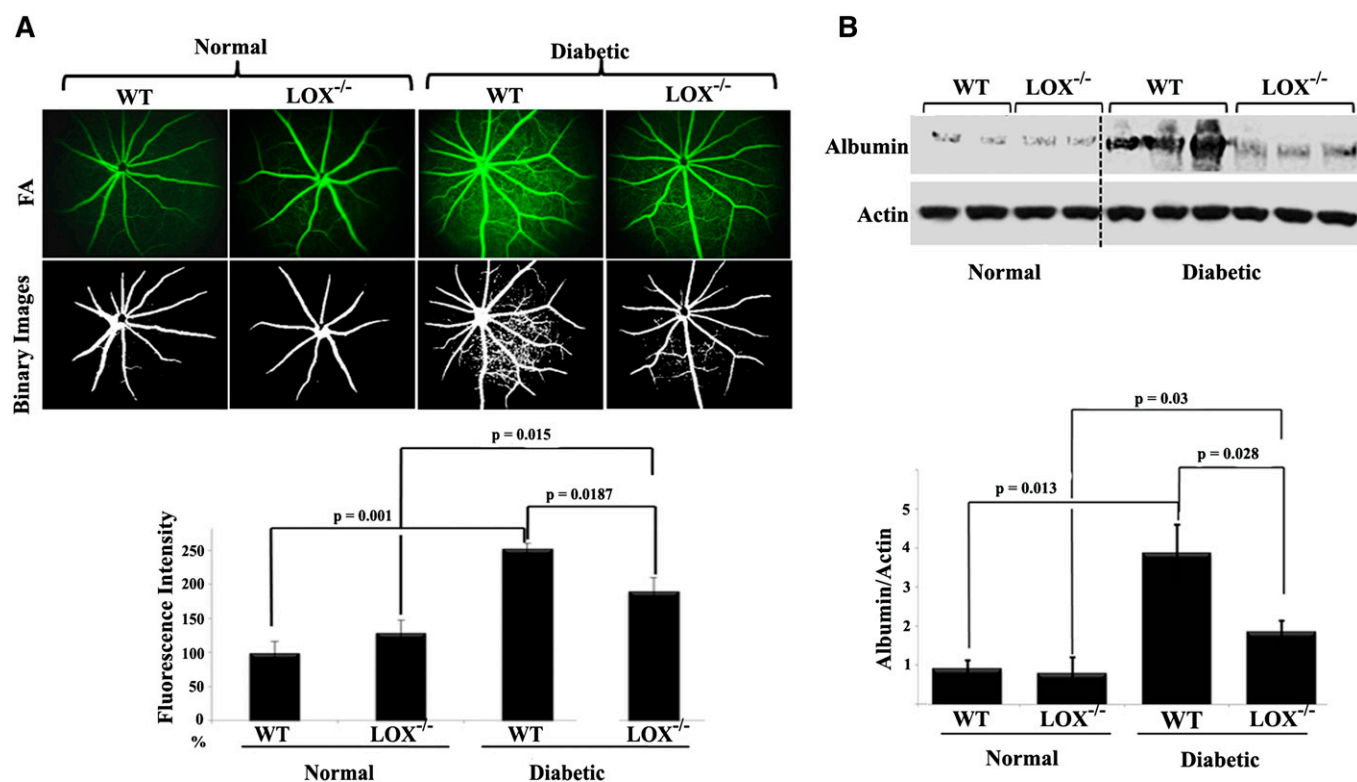


**Fig. 3.** Evolving role of 12/15-LOX in compromising retinal barrier function during diabetes. A: Fluorescein angiography (FA) of normal WT, normal 12/15-LOX<sup>-/-</sup>, diabetic WT, and diabetic 12/15-LOX<sup>-/-</sup> mice together with their binary images. Data are representative pictures taken at constant interval of every mouse studied in each group. The fluorescence intensity of FA per mouse retina was calculated by the ImageJ software after conversion to binary images then normalized to that of normal WT, which was arbitrarily set at 100. B: Western blot of total retinal albumin among the studied groups followed by densitometric analysis. Ratios of albumin band intensities relative to the actin for each group were compared with normal WT control, which was arbitrarily set at 1.0. Data shown for the comparison are the mean  $\pm$  SD of four to six mice studied in each group.

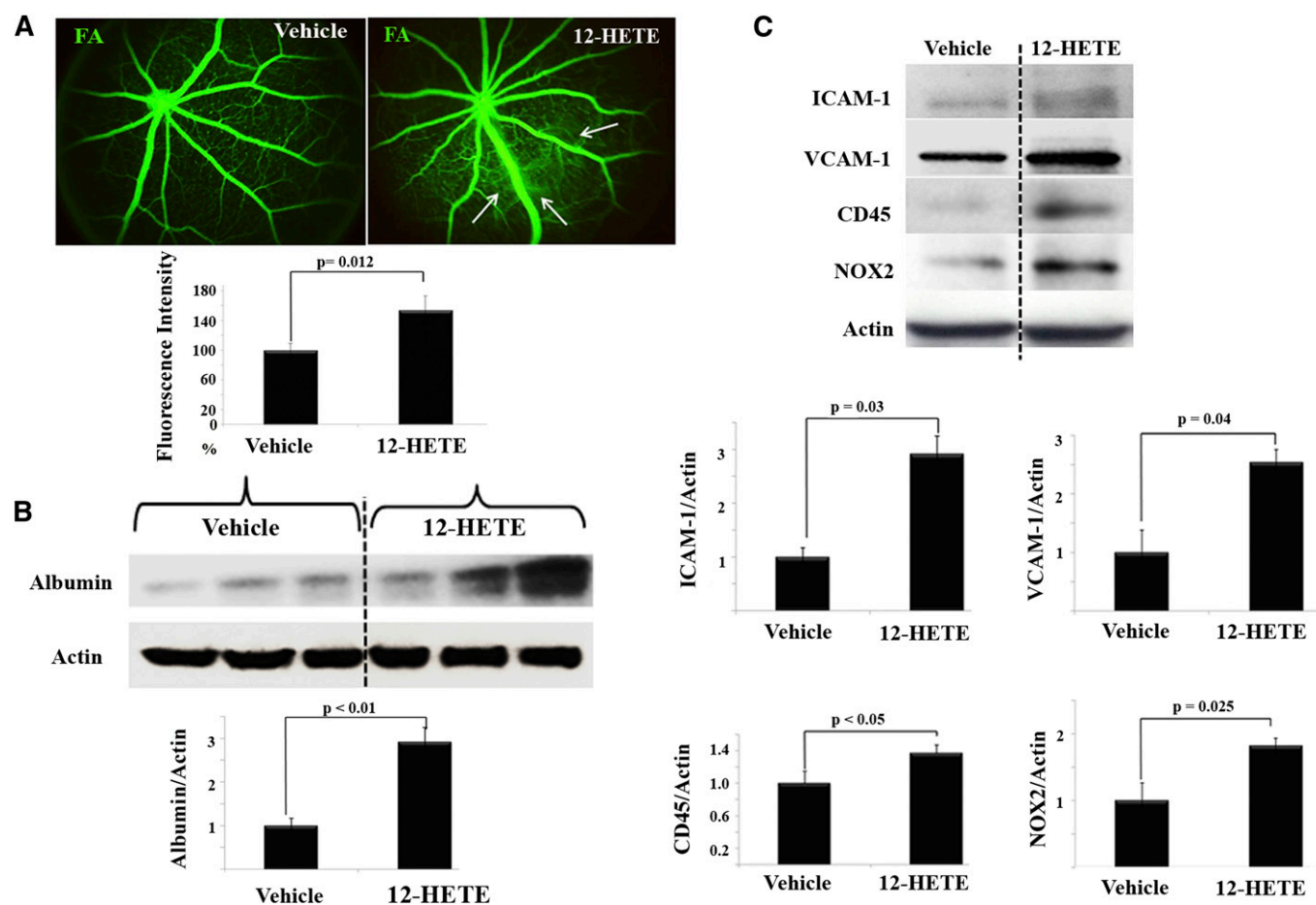


**Fig. 4.** Direct effects of 12/15-LOX-derived metabolites on retinal vasculature. **A:** Fluorescein angiography (FA) of normal WT mice injected intravitreally with vehicle, as a control, or 12-HETE. One week later, FA was performed to evaluate changes of retinal vasculature. The relative fluorescence intensity of FA per mouse retina was calculated by the ImageJ software then normalized as a percentage to that of vehicle-injected control, which was arbitrarily set at 100%. **B:** Western blot of total retinal albumin among the studied groups followed by densitometric analysis. Ratio of the albumin band intensity relative to actin for the 12-HETE-injected group was compared with the vehicle-injected control, which was arbitrarily set at 1.0. **C:** Western blot analysis of retinal ICAM-1, VCAM-1, CD45, and NOX2 after intravitreal injection with either 12-HETE (0.1  $\mu$ M), or vehicle followed by densitometric analysis. Ratios of band intensities of ICAM-1, VCAM-1, CD45, and NOX2, respectively, relative to the actin for 12-HETE-injected group were compared with the vehicle-injected control, which was arbitrarily set at 1.0. Data shown for the comparison are the mean  $\pm$  SD and representative of four to six mice studied in each group.

nondiabetic WT mice. However, knocking out 12/15-LOX resulted in a 59% reduction of total albumin in the retinas of diabetic mice.

Further evidence for the ability of 12/15-LOX to compromise endothelial barrier function was obtained from our second approach. In this approach, an *in vivo* experimental eye model was used in which normal mice were injected intravitreally with a 12/15-LOX-derived predominant murine metabolite, 12-HETE, into the right eye and vehicle into the left eye. Thereafter, the putative biological effect of 12-HETE *per se* on retinal permeability was photographically seen via fluorescein angiography. As shown in **Fig. 4A**, a marked increase in fluorescein leakage was observed in eyes receiving 12-HETE compared with the vehicle-injected contralateral eyes. Concordantly, Western blot analysis for total retinal albumin was performed to further corroborate 12-HETE's ability to induce vascular permeability. As shown in **Fig. 4B**, 12-HETE injection induced a significant 2.8-fold increase in total retinal albumin compared with vehicle-injected controls.

#### The effect of 12-HETE on retinal vasculature was characterized by a marked increase in the inflammatory response

We next sought to determine whether the deleterious effect of 12-HETE on retinal vasculature was associated with a pro-inflammatory phenotype (increased adhesion molecule expression and leukocyte adhesion). To address this point, we determined the effect of 12-HETE injection on retinal levels of ICAM-1 and VCAM-1, well-established markers of endothelial dysfunction in inflammatory conditions (35). Western blot analysis of ICAM-1 showed a 2.9-fold increase in 12-HETE-injected eyes compared with vehicle-injected contralateral eyes. Likewise, the retinal VCAM-1 level was higher (2.5-fold,  $P < 0.05$ ) in 12-HETE-injected eyes than in control. Furthermore, the inflammatory response to the intravitreally injected 12-HETE was determined by leukocyte infiltration as assessed by CD45, a common inflammatory leukocyte antigen. A significant increase in CD45 immunoreactivity (1.4-fold) in the retinas of 12-HETE-injected eyes was observed compared with control (**Fig. 4C**).

### Intravitreal injection of 12-HETE increased retinal expression of NOX2

Previous studies, including those from our laboratory, have pointed out that NOX-derived ROS have a central role in both endothelial and leukocyte activation, keys of the retinal inflammatory paradigm (25, 36). Therefore, a causal relationship between 12-HETE and NOX in mediating endothelial dysfunction was investigated. To accomplish this, we first assessed the question of whether the retinal expression of NOX2 is enhanced by intravitreal injection of 12-HETE or not. As shown in Fig. 4C, the NOX2 protein level was increased 1.7-fold in the retinas of 12-HETE injected eyes compared with contralateral controls, implying an existing causal relationship.

### 12/15-LOX lipid metabolites induce HREC activation/dysfunction in a NOX-dependent manner

Guided by the aforementioned results, the role of the NOX-dependent pathway in 15-HETE-mediated endothelial dysfunction was tested in depth using a cell culture model of HRECs. With this model, incubation with either 12-HETE or 15-HETE significantly activated endothelial

cells to release multiple pro-inflammatory cytokines and chemokines. Among these, IL-6, IL-8, IL-17, and MCP-1 appear to dominate (Fig. 5A). To ensure that 12- or 15-HETE-activated endothelial cells exhibited features of microvascular dysfunction characterized by augmentation of polymorphonuclear leukocyte (PMN) adherence, we performed leukocyte adhesion assays. Exposure of HRECs to 15-HETE for 24 h significantly augmented the number of PMNs adhering to HRECs (5.9-fold increase) compared with control. Next, we tested the role of NOX-derived ROS in 15-HETE-induced leukostasis by using apocynin, a NOX inhibitor, to inhibit ROS generation, as well as NAC (a ROS scavenger) to eliminate ROS as they were generated. When apocynin or NAC was added before 15-HETE, the number of adherent leukocytes induced by 15-HETE dropped back to normal (Fig. 5B). To ensure that these effects were not caused by nonspecific cytotoxicity of apocynin or NAC, we assessed cell viability in HRECs after 24 h exposure to apocynin or NAC, using the MTT assay. Apocynin or NAC, at the concentration used, did not affect HREC viability ( $94 \pm 4\%$  vital cells), indicating that the decrease in the number of adherent leukocytes to

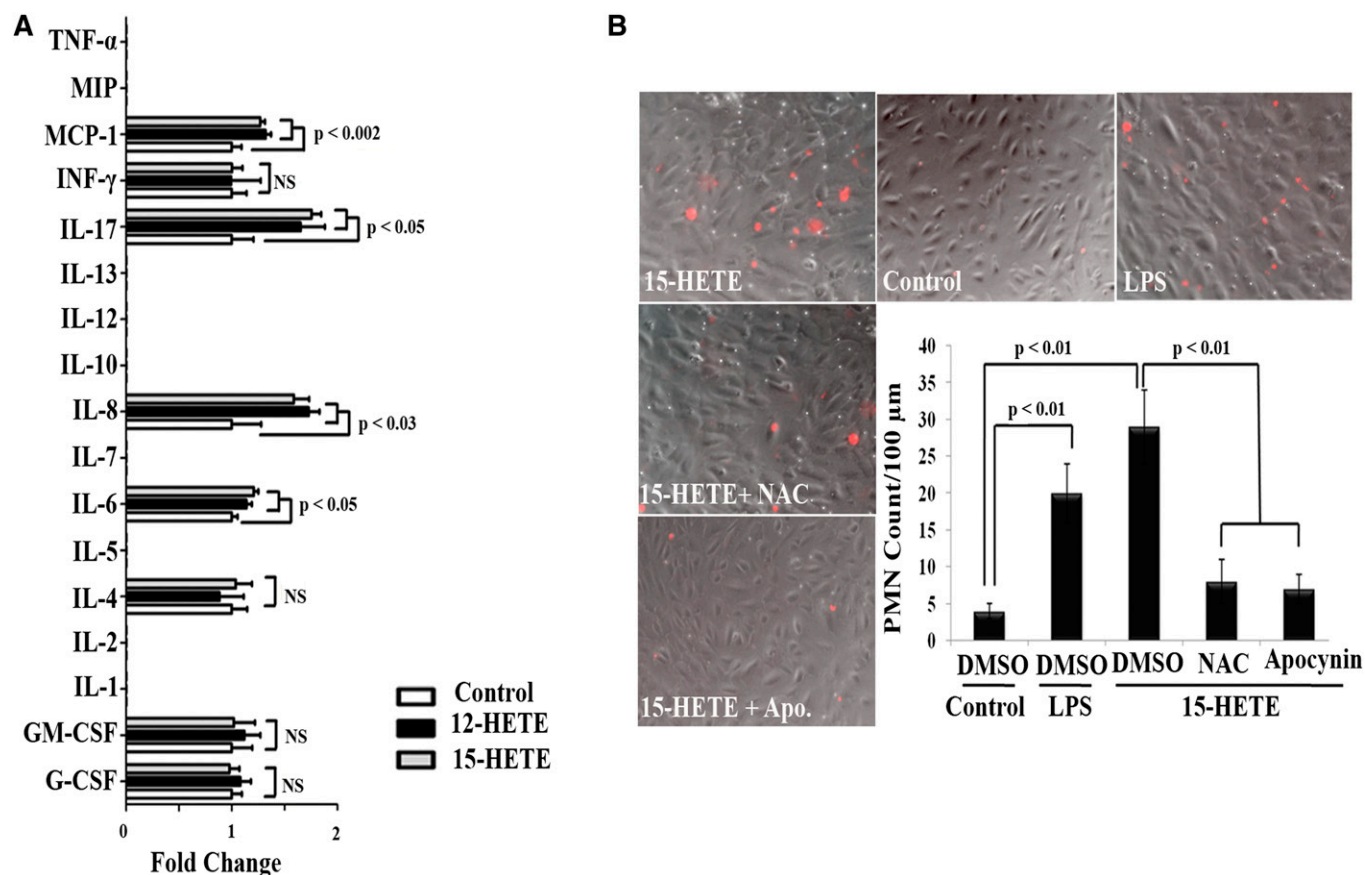


**Fig. 5.** 12-HETE or 15-HETE activates HRECs for leukocyte adhesion in a NOX-dependent manner. A: Multiplex analysis of cytokine and chemokine production in conditioned media of HRECs treated with vehicle or 12- or 15-HETE ( $0.1 \mu\text{M}$ ),  $n = 4$ . B: Reduction of 15-HETE-induced leukocyte adhesion by inhibiting ROS derived from NOX. HRECs were seeded in 24-well plates and treated with 15-HETE ( $0.1 \mu\text{M}$ , 24 h) or vehicle, in the presence or absence of apocynin ( $30 \mu\text{M}$ ) or NAC ( $50 \mu\text{M}$ ). Representative photomicrographs for adherent leukocytes among studied groups; vehicle-treated control, lipopolysaccharide as a positive control, 15-HETE, 15-HETE + apocynin, and 15-HETE + NAC, were taken and quantified for adherent leukocytes. Quantitative data for adherent leukocytes (labeled with red fluorescence dye) were expressed as the mean number of adherent cells per  $100 \mu\text{m} \pm \text{SD}$ . Numbers represent the average of three independent experiments.



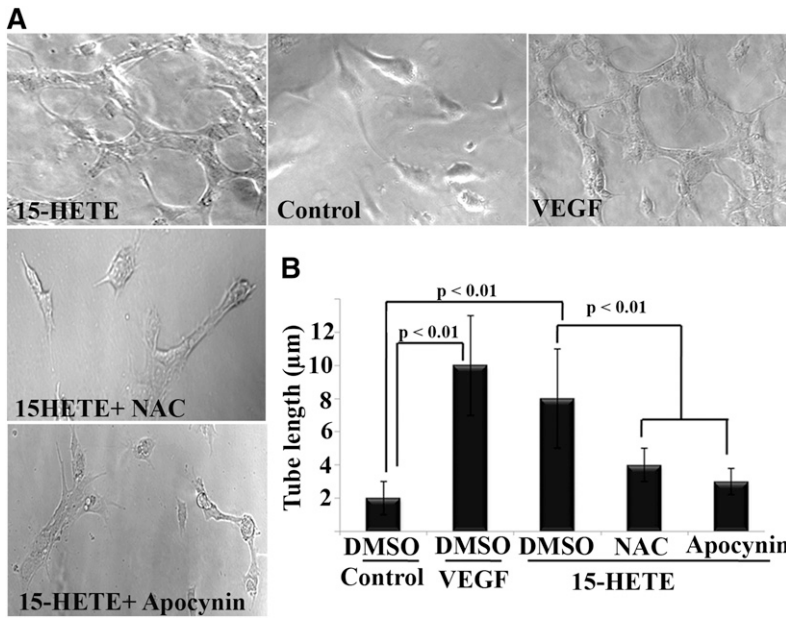


**Fig. 6.** 15-HETE promotes angiogenesis of HRECs through NOX. **A:** Representative photomicrographs for capillary tube formation among studied groups; vehicle-treated control, VEGF as a positive control, 15-HETE, 15-HETE + apocynin, and 15-HETE + NAC. **B:** Quantitative data for endothelial cell tube formation expressed as the mean length of formed tube microns  $\pm$  SD. HRECs were seeded in 96-well plates containing matrigel, and treated with 15-HETE (0.1  $\mu$ M, 24 h) or vehicle, in the presence or absence of apocynin (30  $\mu$ M) or NAC (50  $\mu$ M). Numbers represent average data from three separate experiments.

15-HETE-activated HRECs was indeed consecutive to inhibition of NOX activity, but not to cell death.

In addition to stimulation of leukostasis by 15-HETE, it also promoted retinal endothelial angiogenesis. This is clearly depicted in two representative in vitro angiogenic assays, capillary-like structure formation, and cell migration (Figs. 6, 7). As shown in Fig. 6A and quantified in Fig. 6B, the length of capillary-like structure formed by HRECs in the presence of 15-HETE was significantly increased by 4-fold compared with control. To investigate the contribution of NOX in the formation of capillary-like structure induced by 15-HETE treatment, NOX inhibitors were added to HRECs before 15-HETE treatment. Thereafter, the mean length of tubes between cells was measured. We found that apocynin, as well as NAC, significantly abrogated 15-HETE-induced tube formation. Similarly, 15-HETE significantly increased HREC migration rate, an early step in angiogenesis. This is graphically shown in Fig. 7A, where the capacitance of all treated cells was increased from  $\sim$ 1 nF to 3 nF, wounding phase, then recovered at differential rates during the migration, healing phase. The mean migration rate of HRECs treated with 15-HETE was significantly higher ( $P < 0.01$ ) than the rate obtained with vehicle-treated control. Whether or not NOX is involved in 15-HETE-induced endothelial cell migration was then investigated using two complementary approaches. First, a NOX inhibitor, apocynin, significantly inhibited 15-HETE-induced HREC migration without affecting cell viability (Fig. 7A). Second, HRECs were transiently transfected with NOX2 siRNA or scrambled siRNA (Fig. 7B, C) and then treated with 15-HETE as before. NOX2 siRNA, but not scrambled siRNA, significantly inhibited 15-HETE-induced HREC migration (Fig. 7D).

To further understand the contribution of NOX in mediating endothelial barrier dysfunction induced by 12/15-LOX lipid metabolites, we injected 12-HETE intravitreally into NOX2<sup>-/-</sup> mice. At 1 week after injection, retinal fluorescein leakage of NOX2<sup>-/-</sup> mice was statistically less than

12-HETE-injected WT littermates (Fig. 8). Taken together, these results confirm that NOX is involved in the 12-HETE-induced disruption of the inner BRB integrity.

## DISCUSSION

The current therapeutic interventions to treat DR still rely heavily on controlling systemic hyperglycemia. However, many diabetic patients develop retinopathy despite having a good control (37). Furthermore, the recent targeted treatments strategies, corticosteroids, and anti-VEGF therapies, as well as laser photocoagulation, are limited by their off-target effects. Therefore, it is worthwhile to explore new therapeutic avenues to improve DR. To the best of our knowledge, the current study provides the first preclinical evidence pertaining to the involvement of 12/15-LOX-derived bioactive lipid metabolites in the pathogenesis of vascular barrier breakdown in the early stages of DR. Effectively, our study is the first to screen the bioactive lipid profile in HRECs under hyperglycemic conditions. The key findings of this screen are: 1) The products of the 12/15-LOX pathway were significantly upregulated under hyperglycemic conditions with 15-HETE exhibiting the most significant increase. 2) 15-HETE activates retinal endothelial cells through the NOX system leading to increases in leukocyte adhesion, hyperpermeability, and finally NV, the cardinal signs of DR.

LOX is an enzyme that catalyzes the addition of oxygen to PUFAs containing 1,4-pentadiene structure. The most common analogs are 5-LOX, 12-LOX, and 15-LOX, with the number indicating at which carbon the oxygen is inserted. Of note, species-specific differences between orthologous LOX isoforms have been described for the murine 12-LOX, which is an arachidonate 15-LOX in humans. This difference indicates that care should be taken if experimental data on LOX metabolism are being transferred from one species to another (38, 39). Accordingly,

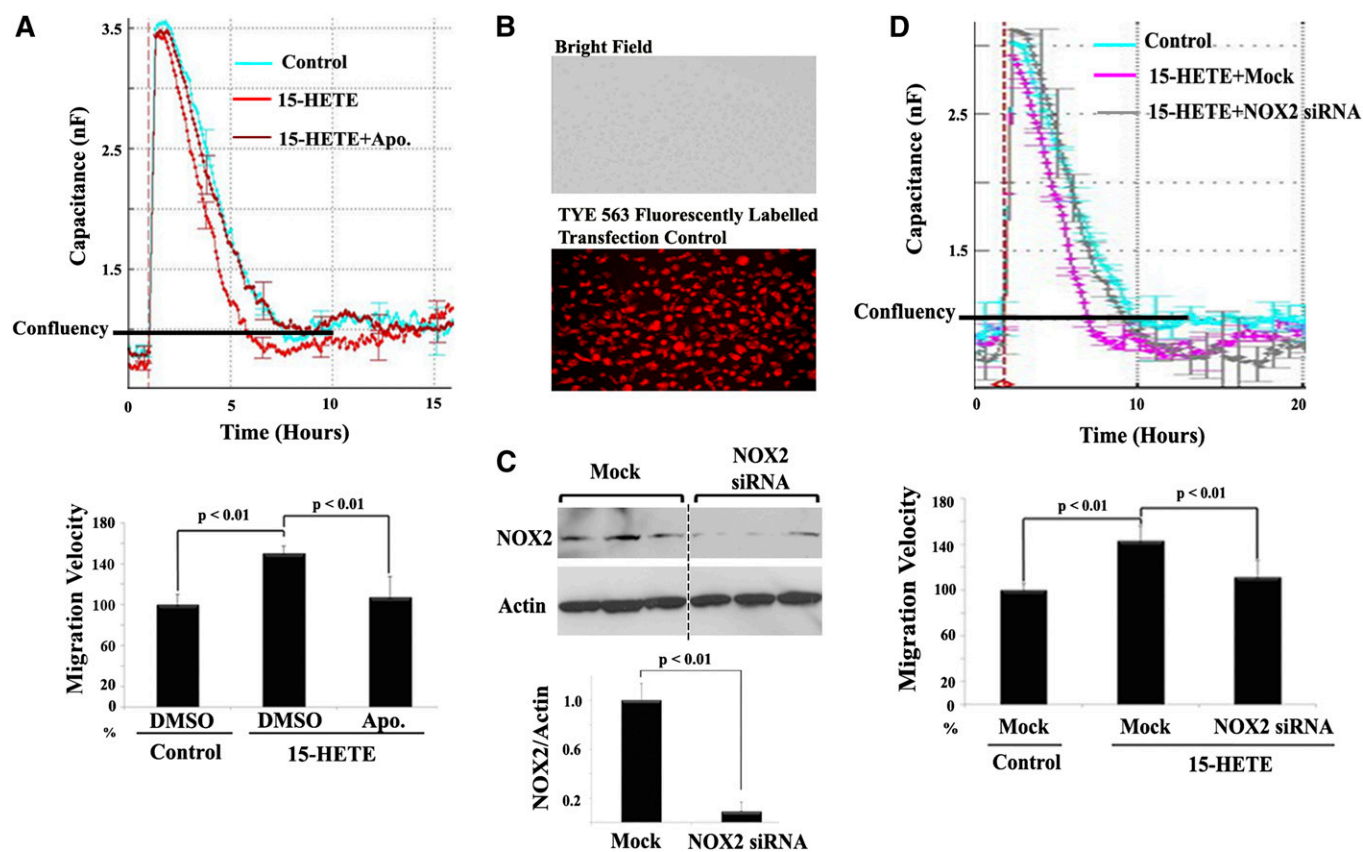


**Fig. 7.** 15-HETE induces HREC migration via NOX-dependent pathway. **A:** Real-time measurement of HREC migration under 15-HETE treatment in the presence of apocynin (Apo.) (30  $\mu$ M) or DMSO using ECIS. The migration velocity was calculated by dividing the total distance that HRECs moved on the radius of the electrode, which is 125  $\mu$ m the time required for recovering 1 nF capacitance, the confluence point, then normalized as a percentage relative to the migration rate obtained from vehicle-treated cells, which was arbitrarily set at 100%. **B–D:** Inhibition of 15-HETE-induced HREC migration by NOX2 siRNA. Cells were transfected with siRNA or scrambled siRNA for 24 h and then treated with 15-HETE for 15 min before wound induction. **B:** Fluorescent detection of transfection control duplex siRNA (TYE 563 fluorescently labeled) in living HRECs 24 h posttransfection. **C:** Measurement of NOX2 expression relative to actin by Western blot after transfection with NOX2 siRNA. **D:** Real-time measurement of HREC migration under 15-HETE treatment in the presence of NOX2 siRNA or scrambled siRNA using ECIS. Relative migration velocity of 15-HETE-treated HRECs in the presence or absence of NOX2 siRNA was normalized as a percentage to that of vehicle with scrambled siRNA-treated cells, which was arbitrarily set at 100%. Data shown are the mean  $\pm$  SD of three independent experiments.

we have used 12-HETE in all murine experiments versus 15-HETE in all human cell experiments. Although a large body of data indicates that LOX plays a role in the pathogenesis of various diseases, including cancer and atherosclerosis, novel physiological roles continue to emerge. In relation to retinal vasculopathies, LOXs present themselves as attractive candidates for therapeutic targeting. This input has originated partly from pathological studies showing the elevated level of 15-HETE in epiretinal membranes of proliferative vitreoretinal and proliferative DR patients (40). These initial observations have been supported by LC/MS analysis of HETEs in biopsied vitreous samples from diabetic subjects (41), and reinforced in postmortem human retinas by additional pathological studies showing a marked increase in the protein levels of both leukocyte and platelet 12/15-LOX in diabetics compared with nondiabetics (21). Furthermore, it has been demonstrated that 5- or 12-LOX deletion reduces diabetes-induced leukostasis. However, deletion of 5-LOX, but not 12-LOX, reduced capillary degeneration (42), suggesting that 5-, 12-, and 15-HETE are each required for

different stages of DR. Additionally, we have previously demonstrated in a model of OIR that 12/15-LOX and its products are important regulators of retinal NV through modulation of VEGF and pigment epithelium-derived factor expression (21). In the present study, we provide evidence for the role of the 12/15-LOX pathway in compromising retinal barrier function early during diabetes. Hence, inhibition of 12/15-LOX could potentially benefit the two main hallmark features of DR, i.e., barrier function disruption and pathological NV, which independently can lead to loss of vision among diabetics.

Next, the direct effects of specific 12/15-LOX-derived metabolites, 12- or 15-HETE, on retinal vasculature were demonstrated by two complementary approaches. First, the intravitreal injection of 12-HETE engendered many of the features characteristic of early DR, including pro-inflammatory response and edema. Second, consistent with previous findings (43), 12- or 15-HETE enhanced several in vitro endothelial cell activities that are relevant to barrier function and angiogenesis, including reduced resistance, adhesion response to PMNs, migration, and tube formation.

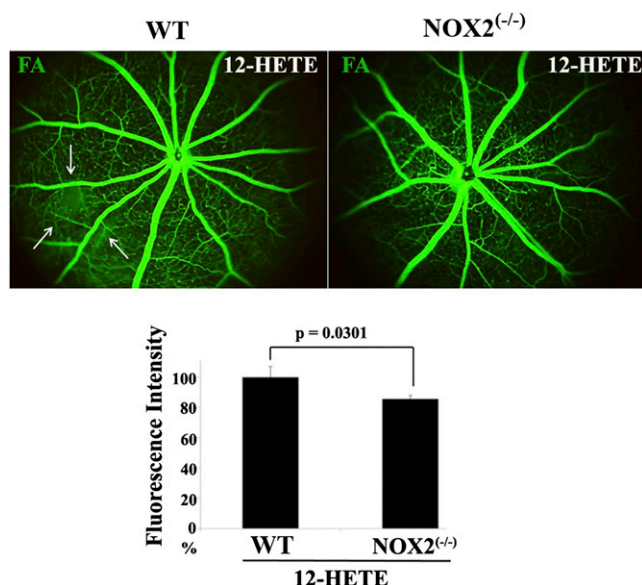


**Fig. 8.** NOX mediates the in vivo deleterious effect of 12-HETE on retinal vasculature. Fluorescein angiography (FA) of normal WT or NOX2<sup>-/-</sup> mice injected intravitreally with 12-HETE. The relative fluorescence intensity of FA per mouse retina was calculated by the ImageJ software and normalized as a percentage to 12-HETE-injected WT mice, arbitrarily set at 100%. Data shown are the mean  $\pm$  SD and representative of four to six mice studied in each group.


Accordingly, the direct relationship between HRECs and eicosanoids has been explored through in vitro study. Previously, Cheranov et al. (44) reported that 15-HETE induced migration and tube formation of HRECs through Src-mediated Rac1 activation. Rac1, in nonphagocytic cells, is a component of the multi-subunit enzyme, NOX, which is composed of the catalytic subunits NOX2 (formerly known as gp91phox) as well as p22phox, and the

cytoplasmic subunits, p47phox and p67phox. Our previous studies using animal and tissue culture models have shown that NOX2 is expressed at low levels in normal retinas and in retinal endothelial cells maintained in control conditions, but is substantially increased in retinal vessels of animals with diabetic or ischemic retinopathy and in retinal endothelial cells exposed to HG or hypoxia (23–26). Furthermore, ROS derived from this enzyme stimulate diverse redox signaling pathways leading to angiogenesis-related gene induction as well as endothelial cell migration and proliferation (45). Therefore, in gaining more insight into the mechanisms of eicosanoid-induced angiogenesis, we expanded upon these studies to portray the causal relationship between NOX and 12- or 15-HETE. Our in vitro studies demonstrated a couple of notable findings: First, the potential angiogenic activity of 12- or 15-HETE in mediating both retinal endothelial cell migration as well as tube formation is regulated in a NOX-dependent manner. Second, we broadened the scope to include other prominent features associated with endothelial dysfunction, such as the secretion of inflammatory cytokines and PMN adhesion. 12-HETE or 15-HETE activates retinal endothelial cells toward a pro-inflammatory phenotype characterized by increased release of IL-6, IL-8, and MCP-1, key regulators of leukocyte recruitment, and the subsequent augmentation of leukocyte adherence through a NOX-dependent mechanism. Together, our results point out that retinal microvascular changes that occur after 12- or 15-HETE challenge are mediated by NOX activity. **Figure 9** illustrates the interplay between these pathways and cross-talk with other cellular processes during DR.

While the introduction of anti-VEGF therapies, ranibizumab and aflibercept, has shifted the treatment paradigm for DR from laser photocoagulation in favor of this targeted approach, there are still major unmet needs and

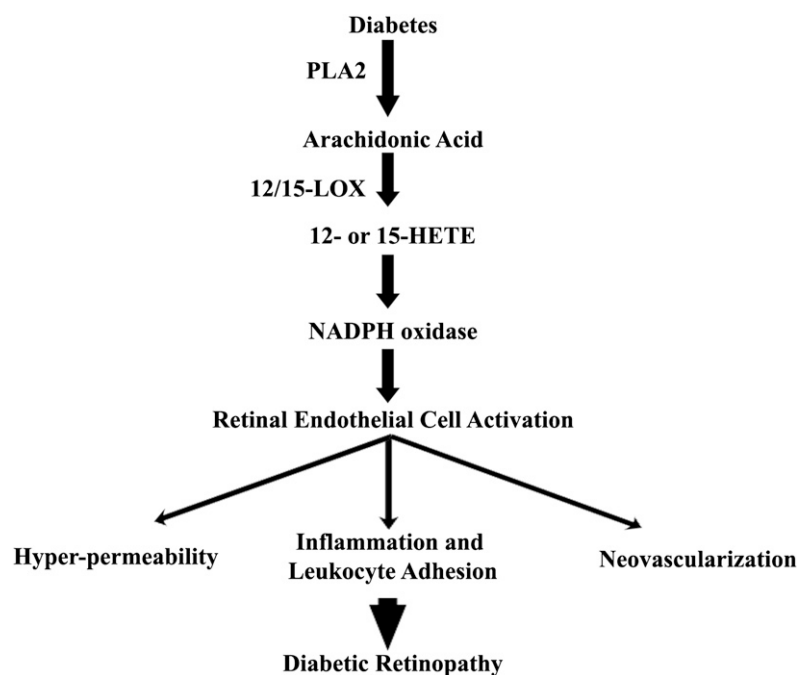


**Fig. 9.** Cascade events involved in the pathogenesis of DR: Hyperglycemia activates the PLA2 to release AA from the retinal cell membrane. AA is then converted to 12- or 15-HETE that generates ROS through NOX, creating a status of oxidative stress. This oxidative stress leads to the activation of retinal endothelial cells through various inflammatory signaling pathways, leading to leukocyte adhesion, hyperpermeability, and ultimately NV (the cardinal signs of DR).

gaps in the understanding of underlying biological processes. The potential long-term consequences of intraocular VEGF suppression on the retina have to be taken into account, because VEGF is a survival factor for retinal neurons (46). Thereby, targeting a pathway that has crucial roles in compromising the vascular integrity in early DR would provide long-term retinal vascular benefits without affecting neighboring neurons. Our current and previous studies (22) suggest 12/15-LOX as a potential therapeutic target that mediates microvascular dysfunction in DR, probably via a NOX-dependent mechanism. Therefore, inhibition of the activated retinal 12/15-LOX system would allow the occurrence of a baseline level of VEGF to exert its direct neuroprotective effects and thus might provide a therapeutic strategy in modulating pathological pathways of DR when the VEGF level is not correlated with disease severity. 

The authors would like to thank Dr. Krishna Maddipati for his assistance with the lipid analysis and discussion.

## REFERENCES

- Fong, D. S., L. P. Aiello, F. L. Ferris III, and R. Klein. 2004. Diabetic retinopathy. *Diabetes Care*. **27**: 2540–2553.
- Frank, R. N. 2004. Diabetic retinopathy. *N. Engl. J. Med.* **350**: 48–58.
- Jeganathan, V. S. 2011. Anti-angiogenesis drugs in diabetic retinopathy. *Curr. Pharm. Biotechnol.* **12**: 369–372.
- Quaggin, S. E. 2012. Turning a blind eye to anti-VEGF toxicities. *J. Clin. Invest.* **122**: 3849–3851.
- Falavarjani, K. G., and Q. D. Nguyen. 2013. Adverse events and complications associated with intravitreal injection of anti-VEGF agents: a review of literature. *Eye (Lond.)*. **27**: 787–794.
- Elman, M. J., N. M. Bressler, H. Qin, R. W. Beck, F. L. Ferris III, S. M. Friedman, A. R. Glassman, I. U. Scott, C. R. Stockdale, and J. K. Sun; Diabetic Retinopathy Clinical Research Network. 2011. Expanded 2-year follow-up of ranibizumab plus prompt or deferred laser or triamcinolone plus prompt laser for diabetic macular edema. *Ophthalmology*. **118**: 609–614.
- Han, D. P., and D. K. Heuer. 2012. Intravitreal corticosteroid therapy: putting the problem of glaucoma in perspective. *Arch. Ophthalmol.* **130**: 380–382.
- Akduman, L., and R. J. Olk. 1997. Laser photocoagulation of diabetic macular edema. *Ophthalmic Surg. Lasers*. **28**: 387–408.
- Sacks, F. M., M. P. Hermans, P. Fioretto, P. Valensi, T. Davis, E. Horton, C. Wanner, K. Al-Rubeaan, R. Aronson, I. Barzon, et al. 2014. Association between plasma triglycerides and high-density lipoprotein cholesterol and microvascular kidney disease and retinopathy in type 2 diabetes mellitus: a global case-control study in 13 countries. *Circulation*. **129**: 999–1008.
- Malek, M., M. E. Khamseh, R. Aghili, Z. Emami, L. Najafi, and H. R. Baradaran. 2012. Medical management of diabetic retinopathy: an overview. *Arch. Iran Med.* **15**: 635–640.
- Lupo, G., C. Motta, G. Giurdanella, C. D. Anfuso, M. Alberghina, F. Drago, S. Salomone, and C. Bucolo. 2013. Role of phospholipases A2 in diabetic retinopathy: in vitro and in vivo studies. *Biochem. Pharmacol.* **86**: 1603–1613.
- Morita, I., R. Takahashi, H. Ito, H. Orimo, and S. Murota. 1983. Increased arachidonic acid content in platelet phospholipids from diabetic patients. *Prostaglandins Leukot. Med.* **11**: 33–41.
- Lagarde, M. 2005. Book Review: Bioactive Lipids. Edited by Anna Nicolaou and George Kokotos. *Eur. J. Lipid Sci. Technol.* **107**: 272.
- Evans, J. F., and J. H. Hutchinson. 2010. Seeing the future of bioactive lipid drug targets. *Nat. Chem. Biol.* **6**: 476–479.
- Chang, Y. C., and W. C. Wu. 2013. Dyslipidemia and diabetic retinopathy. *Rev. Diabet. Stud.* **10**: 121–132.
- Kühn, H., and V. B. O'Donnell. 2006. Inflammation and immune regulation by 12/15-lipoxygenases. *Prog. Lipid Res.* **45**: 334–356.
- Brash, A. R. 1999. Lipoxygenases: occurrence, functions, catalysis, and acquisition of substrate. *J. Biol. Chem.* **274**: 23679–23682.
- Bajpai, A. K., E. Blaskova, S. B. Pakala, T. Zhao, W. C. Glasgow, J. S. Penn, D. A. Johnson, and G. N. Rao. 2007. 15(S)-HETE production in human retinal microvascular endothelial cells by hypoxia: novel role for MEK1 in 15(S)-HETE induced angiogenesis. *Invest. Ophthalmol. Vis. Sci.* **48**: 4930–4938.
- Chu, H. W., S. Balzar, J. Y. Westcott, J. B. Trudeau, Y. Sun, D. J. Conrad, and S. E. Wenzel. 2002. Expression and activation of 15-lipoxygenase pathway in severe asthma: relationship to eosinophilic phenotype and collagen deposition. *Clin. Exp. Allergy*. **32**: 1558–1565.
- Li, J., J. Rao, Y. Liu, Y. Cao, Y. Zhang, Q. Zhang, and D. Zhu. 2013. 15-Lipoxygenase promotes chronic hypoxia-induced pulmonary artery inflammation via positive interaction with nuclear factor-kappaB. *Arterioscler. Thromb. Vasc. Biol.* **33**: 971–979.
- Al-Shabrawey, M., R. Mussell, K. Kahook, A. Tawfik, M. Eladl, V. Sarthy, J. Nussbaum, A. El-Marakby, S. Y. Park, Z. Gurel, et al. 2011. Increased expression and activity of 12-lipoxygenase in oxygen-induced ischemic retinopathy and proliferative diabetic retinopathy: implications in retinal neovascularization. *Diabetes*. **60**: 614–624.
- Othman, A., S. Ahmad, S. Megyerdi, R. Mussell, K. Choksi, K. R. Maddipati, A. Elmarakby, N. Rizk, and M. Al-Shabrawey. 2013. 12/15-Lipoxygenase-derived lipid metabolites induce retinal endothelial cell barrier dysfunction: contribution of NADPH oxidase. *PLoS ONE*. **8**: e57254.
- Al-Shabrawey, M., M. Bartoli, A. B. El-Remessy, G. Ma, S. Matragoon, T. Lemtalsi, R. W. Caldwell, and R. B. Caldwell. 2008. Role of NADPH oxidase and Stat3 in statin-mediated protection against diabetic retinopathy. *Invest. Ophthalmol. Vis. Sci.* **49**: 3231–3238.
- Al-Shabrawey, M., M. Bartoli, A. B. El-Remessy, D. H. Platt, S. Matragoon, M. A. Behzadian, R. W. Caldwell, and R. B. Caldwell. 2005. Inhibition of NAD(P)H oxidase activity blocks vascular endothelial growth factor overexpression and neovascularization during ischemic retinopathy. *Am. J. Pathol.* **167**: 599–607.
- Al-Shabrawey, M., M. Rojas, T. Sanders, A. Behzadian, A. El-Remessy, M. Bartoli, A. K. Parpia, G. Liou, and R. B. Caldwell. 2008. Role of NADPH oxidase in retinal vascular inflammation. *Invest. Ophthalmol. Vis. Sci.* **49**: 3239–3244.
- Tawfik, A., T. Sanders, K. Kahook, S. Akeel, A. Elmarakby, and M. Al-Shabrawey. 2009. Suppression of retinal peroxisome proliferator-activated receptor gamma in experimental diabetes and oxygen-induced retinopathy: role of NADPH oxidase. *Invest. Ophthalmol. Vis. Sci.* **50**: 878–884.
- Ibrahim, A. S., A. B. El-Remessy, S. Matragoon, W. Zhang, Y. Patel, S. Khan, M. M. Al-Gayyar, M. M. El-Shishtawy, and G. I. Liou. 2011. Retinal microglial activation and inflammation induced by amadori-glycated albumin in a rat model of diabetes. *Diabetes*. **60**: 1122–1133.
- Remtulla, S., and P. E. Hallett. 1985. A schematic eye for the mouse, and comparisons with the rat. *Vision Res.* **25**: 21–31.
- Ibrahim, A. S., M. A. Sobh, H. M. Eid, A. Salem, H. H. Elbelasi, M. H. El-Naggar, F. M. AbdelBar, H. Sheashaa, M. A. Sobh, and F. A. Badria. 2014. Gingerol-derivatives: emerging new therapy against human drug-resistant MCF-7. *Tumour Biol.* **35**: 9941–9948.
- Hussein, K. A., K. Choksi, S. Akeel, S. Ahmad, S. Megyerdi, M. El-Sherbiny, M. Nawaz, A. Abu El-Asrar, and M. Al-Shabrawey. 2014. Bone morphogenetic protein 2: A potential new player in the pathogenesis of diabetic retinopathy. *Exp. Eye Res.* **125**: 79–88.
- Chan, C. M., J. Y. Fang, H. H. Lin, C. Y. Yang, and C. F. Hung. 2009. Lycopene inhibits PDGF-BB-induced retinal pigment epithelial cell migration by suppression of PI3K/Akt and MAPK pathways. *Biochem. Biophys. Res. Commun.* **388**: 172–176.
- Maddipati, K. R., R. Romero, T. Chaiworapongsa, S. L. Zhou, Z. Xu, A. L. Tarca, J. P. Kusanovic, H. Munoz, and K. V. Honn. 2014. Eicosanomic profiling reveals dominance of the epoxygenase pathway in human amniotic fluid at term in spontaneous labor. *FASEB J.* **28**: 4835–4846.
- Tawfik, A., S. Markand, M. Al-Shabrawey, J. N. Mayo, J. Reynolds, S. E. Bearden, V. Ganapathy, and S. B. Smith. 2014. Alterations of retinal vasculature in cystathionine- $\beta$ -synthase heterozygous mice: a model of mild to moderate hyperhomocysteinemia. *Am. J. Pathol.* **184**: 2573–2585.
- Nagata, D., M. Mogi, and K. Walsh. 2003. AMP-activated protein kinase (AMPK) signaling in endothelial cells is essential for angiogenesis in response to hypoxic stress. *J. Biol. Chem.* **278**: 31000–31006.
- Videm, V., and M. Albrigtsen. 2008. Soluble ICAM-1 and VCAM-1 as markers of endothelial activation. *Scand. J. Immunol.* **67**: 523–531.

36. Nwariaku, F. E., Z. Liu, X. Zhu, D. Nahari, C. Ingle, R. F. Wu, Y. Gu, G. Sarosi, and L. S. Terada. 2004. NADPH oxidase mediates vascular endothelial cadherin phosphorylation and endothelial dysfunction. *Blood*. **104**: 3214–3220.
37. Zhang, L., G. Krzentowski, A. Albert, and P. J. Lefebvre. 2001. Risk of developing retinopathy in Diabetes Control and Complications Trial type 1 diabetic patients with good or poor metabolic control. *Diabetes Care*. **24**: 1275–1279.
38. Kuhn, H. 2004. Lipoxygenases in the cardiovascular system. *Circ. Res.* **94**: 1527–1529.
39. Funk, C. D., X. S. Chen, E. N. Johnson, and L. Zhao. 2002. Lipoxygenase genes and their targeted disruption. *Prostaglandins Other Lipid Mediat.* **68–69**: 303–312.
40. Augustin, A. J., F. H. Grus, F. Koch, and M. Spitznas. 1997. Detection of eicosanoids in epiretinal membranes of patients suffering from proliferative vitreoretinal diseases. *Br. J. Ophthalmol.* **81**: 58–60.
41. Schwartzman, M. L., P. Iserovich, K. Gotlinger, L. Bellner, M. W. Dunn, M. Sartore, M. Grazia Pertile, A. Leonardi, S. Sathe, A. Beaton, et al. 2010. Profile of lipid and protein autacoids in diabetic vitreous correlates with the progression of diabetic retinopathy. *Diabetes*. **59**: 1780–1788.
42. Gubitosi-Klug, R. A., R. Talahalli, Y. Du, J. L. Nadler, and T. S. Kern. 2008. 5-Lipoxygenase, but not 12/15-lipoxygenase, contributes to degeneration of retinal capillaries in a mouse model of diabetic retinopathy. *Diabetes*. **57**: 1387–1393.
43. Graeber, J. E., B. M. Glaser, B. N. Setty, J. A. Jerdan, R. W. Walenga, and M. J. Stuart. 1990. 15-Hydroxyeicosatetraenoic acid stimulates migration of human retinal microvessel endothelium in vitro and neovascularization in vivo. *Prostaglandins*. **39**: 665–673.
44. Cheranov, S. Y., D. Wang, V. Kundumani-Sridharan, M. Karpurapu, Q. Zhang, K. R. Chava, and G. N. Rao. 2009. The 15(S)-hydroxyeicosatetraenoic acid-induced angiogenesis requires Janus kinase 2-signal transducer and activator of transcription-5B-dependent expression of interleukin-8. *Blood*. **113**: 6023–6033.
45. Li, N., and M. Karin. 1999. Is NF-kappaB the sensor of oxidative stress? *FASEB J.* **13**: 1137–1143.
46. Saint-Geniez, M., A. S. Maharaj, T. E. Walshe, B. A. Tucker, E. Sekiyama, T. Kurihara, D. C. Darland, M. J. Young, and P. A. D'Amore. 2008. Endogenous VEGF is required for visual function: evidence for a survival role on muller cells and photoreceptors. *PLoS ONE*. **3**: e3554.